Climate Dynamics
https://doi.org/10.1007/s00382-018-4131-5

Relationship between the onset date of the Meiyu and the South Asian anticyclone in April and the related mechanisms

Hua Li[1,2,3] · **Shengping He**[1,4] · **Ke Fan**[1,5] · **Huijun Wang**[1,2,5]

Received: 29 June 2017 / Accepted: 7 February 2018
© Springer-Verlag GmbH Germany, part of Springer Nature 2018

Abstract
The onset date of the Meiyu has attracted extensive attention because it marks the beginning of the rainfall season in the Yangtze-Huai River basin (YHRB). In this study, the relationship between the onset dates of the Meiyu and its precursors is investigated; and the South Asian anticyclone (SAA) in April, which is generated by atmospheric apparent sources over South Asia, is introduced. The results show that years with stronger SAA in April are concurrent with earlier onsets of the Meiyu and increased precipitation in June over the YHRB and vice versa. The mechanisms involved in this relationship are further investigated. The SAA emerges in early April, and moves eastward to the western North Pacific (WNP) in the late pentad of April due to the abrupt zonal energy transport, leading to anomalous divergence in the upper troposphere over the WNP. The divergence anomaly enhances ascending motion in situ due to Ekman pumping, leading to an anomalous cyclone at lower levels over this region. Due to the southward-moving ascending motion and the presence of the lower tropospheric cyclone in the fourth pentad of May, the precipitation moves southward to the Philippine Sea (PHS). The associated stronger convection over the PHS further triggers a meridional overturning pattern, which develops into the Pacific-Japan like pattern (PJ-like pattern). The PJ-like pattern persists from the end of May to the beginning of June, which promotes the earlier onset of the Meiyu. In addition, due to the increased heating associated with the abundant precipitation over the PHS around the fourth pentad of May, the Western Pacific subtropical high (WPSH) shifts northward earlier. Ultimately, the earlier establishment of the PJ-like pattern and the earlier northward shift of the WPSH cause stronger-than-normal southwesterly flows and additional water vapor transport to the YHRB, leading to the advanced onset of the Meiyu and additional precipitation in June.

Keywords Meiyu onset date · South Asian anticyclone · Philippines Sea · Pacific-Japan like pattern

1 Introduction

Over East Asia, the rainy season is strongly influenced by the summer monsoon. The rain season is called the Meiyu in China, the Baiu in Japan, and Changma in Korea (Tao and Chen 1987). It has profound impacts on agriculture, water resources, human activities and socioeconomic activities in the Meiyu region, which is the most densely populated region in East Asia. Regarding China, the Meiyu precipitation usually accounts for more than 20% of the annual precipitation, and this fraction sometimes exceeds 50% in the Meiyu region (28°–34°N, 110°−122°E, Wang et al. 2005). Therefore, to a certain extent, anomalous precipitation during Meiyu periods, especially anomalies in the intensity and location of the Meiyu belt, can lead to natural disasters in this area (Chen and Chang 1980; Lau et al. 1988; Ding 1992; Chang 2004; Zhou et al. 2009). In general, the main Meiyu in China appears in the middle of June and withdraws

✉ Hua Li
lihua@mail.iap.ac.cn

1 Nansen-Zhu International Research Centre, Institute of Atmospheric Physics, Chinese Academy of Sciences, Beijing, China

2 Climate Change Research Center, Chinese Academy of Sciences, Beijing, China

3 University of Chinese Academy of Sciences, Beijing, China

4 Geophysical Institute, University of Bergen, Bjerknes Centre for Climate Research, Bergen 5007, Norway

5 Collaborative Innovation Center on Forecast and Evaluation of Meteorological Disasters, Key Laboratory of Meteorological Disaster, Ministry of Education, Nanjing University of Information Science and Technology, Nanjing, China

Published online: 01 March 2018

in early July, and the average length of the Meiyu period is approximately 21 days (Ding 1992; Ding et al. 2007). These are vital parameters for the Meiyu and have an evident interannual variability (Ding et al. 2007). The onset and withdrawal dates determine the length of the Meiyu, which is closely related to the amount of precipitation during the Meiyu period. Thus, the study of the onset and withdrawal date of the Meiyu is important for understanding the anomalous precipitation and for disaster prevention and water resource management in the Meiyu region.

A large number of papers have investigated the Meiyu based on its climatological characteristics and homochronous atmospheric circulation (e.g., Tao and Chen 1987; Ding 1992; Ding et al. 2007; Huang et al. 2011). The configuration of atmospheric circulation from the lower to upper troposphere is characterized by distinct features during the Meiyu, for instance, the South Asian High (SAH) and the westerly jet stream in the upper troposphere and blocking in the middle troposphere and Western Pacific subtropical high (WPSH) at lower levels. These synoptic systems have important impacts on Meiyu precipitation (Akiyama 1973; Chen and Yu 1988; Kodama 1992). On the other hand, numerous studies have addressed the dynamic structure of the Meiyu front and regard the Meiyu as a mesoscale weather phenomenon (Chen 1983; Krishnan and Sugi 2001; Ninomiya and Shibagaki 2007; Wakazuki et al. 2006; Yu et al. 2012). Those studies suggest that the Meiyu front is quasi-stationary and can generate long clouds and rainbands with mesoscale disturbances embedded within them. In addition, several previous studies have emphasized the interannual or interdecadal changes in precipitation. For example, Zhu et al. (2013) found that the two types of El Niño-Southern Oscillation (ENSO) have different impacts on Meiyu precipitation and addressed the physical linking of the decadal changes that occurred in approximately 1991. Zhu et al. (2011, 2015) revealed a decadal change in the summer precipitation in the Huang-Huai River and the Yangtze River region in the 2000s and its relationship with the shifts in the Pacific Decadal Oscillation to a negative phase. Recently, Sampe and Xie (2010) noted that the westerly jet plays a key role in stimulating and maintaining the Meiyu rainbands. Li and Zhang (2014) further described that the different configurations of the subtropical and polar front jets have different influences on the precipitation amount and location of the Meiyu rain belts.

Previous investigations have also suggested that the abrupt change in atmospheric circulation from winter to summer patterns in Asia is closely connected to the onset of the Meiyu in China (Yeh et al. 1959; Tao and Chen 1987), which means that the atmospheric circulations associated with the onset of the Meiyu might have a close connection to its previous stage and evolutionary process. Some particular atmospheric circulations or systems in the early period may play an important role in the onset of the Meiyu and may be useful for predicting the onset of the Meiyu.

Numerous studies in the literature have described the onset of the Meiyu and the associated factors (Lu et al. 2001). However, only a few studies have paid attention to the precursor circulations that are related to the onset of the Meiyu (e.g., Zhang et al. 2005; Zhu et al. 2008), leading to a poor understanding of the precursory synoptic systems or large-scale characteristics connected with the onset of the Meiyu. Recent studies of the onset of Meiyu have usually focused on the following aspects. (1) Different large-scale atmospheric circulations occur in years with the early and late onset of the Meiyu period. For example, Lu et al. (2001) found that the East Asia westerly jets and subtropical highs display evident differences and different onset dates, but similar studies have not found enough precursor signals to make short-term forecasts. (2) Several studies have looked for precursor signals. Zhu et al. (2008) described that Meiyu onsets may be associated with the ENSO. Choi et al. (2012) defined a new Changma onset index and indicated its connection with the Antarctic Oscillation. Recently, Park et al. (2015) built a statistical prediction model for the Changma onset based on dynamical methods, and the prediction model consisted of several precursory factors identified using traditional statistical methods. However, considering that the onset of the Meiyu has large interannual variability and is complicated, its prediction at seasonal and interseasonal scales remains difficult. Regarding short-term climate forecasts, the challenges are mainly reflected in finding and addressing the mechanisms. Therefore, it is particularly important to seek the precursory factors as many as possible, especially those factors that are independent of each other. The primary purposes of this research, therefore, are to investigate the association of a precursory climate system with the onset of the Meiyu and to address its internal physical mechanisms. Finally, it is expected that this study will provide a foundation for further understanding the Meiyu changes and increase the skill of short-term climate forecasts of the Meiyu.

The paper is organized as follows. In Sect. 2, we provide a brief review of the datasets and the definition of the Meiyu onset date used in this analysis. In Sect. 3, we review the South Asian anticyclone (SAA) in April and its dynamic origin and further describe its statistical relationship with the onset of the Meiyu. In Sect. 4, we discuss the impacts of circulations related to the SAA in April on the Meiyu onset. The possible mechanisms on the relationship between the SAA and onset of the Meiyu are given in Sect. 5. Finally, Sect. 6 provides a summary of the key results and a brief discussion of aspects of the issues that are worthy of study but beyond the scope of this study.

2 Data and methods

2.1 Dataset

Several datasets were used in this study, which spans the period from 1979 to 2014, including (1) daily and monthly atmospheric variables from National Centers for Environmental Prediction/National Center for Atmospheric Research (NCEP/NCAR) reanalysis (Kalnay et al. 1996), (2) the pentad and monthly Climate Prediction Center (CPC) Merged Analysis of Precipitation (CMAP) data (Xie and Arkin 1996), (3) a daily precipitation dataset from 756 stations in China, which was supplied by the National Meteorological Information Center of the China Meteorological Administration, and (4) daily mean interpolated outgoing longwave radiation (OLR) data measured by a National Oceanic and Atmospheric Administration (NOAA) satellite for the period 1979–2013 (Liebmann and Smith 1996).

2.2 Methods

The onset dates of the Meiyu were determined using precipitation data from the five selected stations [Wuhan (30°37′N, 114°08′E), Nanjing (32°00′N, 118°48′E), Wuhu (31°20′N, 118°23′E), Jiujiang (29°44′N, 116°00′E) and Shanghai (31°24′N, 121°27′E)]. Missing precipitation data from any station were assigned by interpolation using data from nearby stations, which are sparsely distributed within the Meiyu region, as well as the position of the WPSH ridge. Days when the daily precipitation at more than two stations among the five selected stations exceeded 0.1 mm and the total precipitation at the five stations exceeded 10 mm were referred to as rainy days in the Meiyu region. If rainy days during a period from the first rainy day to the subsequent 10 days exceeded 5 days, and the position of the WPSH ridge was located within the latitude band that extends from 20°N to 25°N, the first rainy day was assigned as the onset date of the Meiyu. The Meiyu region was confined to 28°N–34°N and 110°E–122°E, according to the definition in Ding et al. (2007).

3 Variability of the Meiyu onset and the South Asian anticyclone

We first calculated the onset dates of the Meiyu during 1979 to 2014 using the method defined by Ding et al. (2007), and the dates indicate the beginning of the rainfall reason in the YHRB. The time series is shown in Fig. 1b. The values plotted on the vertical ordinate are the onset dates and positive (negative) values greater (less) than or equal to + (−) 0.5 standard deviation correspond to earlier (later) onsets of the Meiyu. The average onset date during 1979 to 2014 was approximately 18 June (Table 1). A notable characteristic is that the time series of the onset dates mainly show large interannual variability. As mentioned in Sect. 1, the early stage circulations may play a key role in the onset of the Meiyu. To detect the potential connection of the Meiyu with the preceding climatic systems, we calculated the regression circulations in previous stages onto the Meiyu onset date. It was found that the anticyclone at 200 hPa over South Asian in April showed the most significant positive relationship with the Meiyu onset date. As shown in Fig. 1a, it is apparent that there was an anomalous anticyclone over South Asia in April that was associated with the earlier start of the Meiyu. The anomalous anticyclone extended from 300 to 100 hPa and had a quasi-barotropic structure in the upper troposphere (not shown). However, a crucial question appears: is the anticyclone significant mode or merely a part of random variability? To answer the question, the multivariate empirical orthogonal function (MV-EOF) analysis was employed to verify its robustness. The MV-EOF analysis method was described in detail by Wang (1992) and it has been widespread used in atmospheric analysis (e.g., Wang et al. 2008; Xu et al. 2016). In this paper, an area-weighted correlation coefficient matrix was constructed for the combined zonal and meridional winds to carry out the MV-EOF. The first MV-EOF mode (MV-EOF1) is shown in Fig. 1c, it accounts for 15.4% of the total variance and the pattern is similar to the anticyclone revealed by regression (Fig. 1a, c). Additionally, the MV-EOF1 is statistically distinguished from the rest of the modes according to the rule given by North et al. (1982). It should be noted that the MV-EOF1 is insensitive with the region size chosen for the EOF analysis. Furtherly, to quantitatively demonstrate the anticyclone, we defined an index in terms of the area-averaged negative vorticity at 200 hPa over the region (10°N–30°N, 80°E–120°E), which is referred as SAAI. As shown in Fig. 1d, the standardized SAAI and time series of MV-EOF1 coincide with each other, with a correlation coefficient of 0.85 (above the 99% confidence level estimated by Student's *t* test). Thus, the anticyclone in the upper troposphere is a significant mode in April.

Due to the system is located in South Asia at upper troposphere, it is necessary to examine the relation between the SAA and the SAH. Therefore, a SAH index (SAHI) in April was further defined as the area-averaged vorticity over the region (0°N–20°N, 100°E–160°E), where the climatologic SAH is located (Reiter and Gao 1982). The correlation coefficient between SAAI and SAHI is 0.02, suggesting that the two system are independent. To fourthly understand the dynamic fundamental of the SAA and also to examine its difference from the SAH. The regression homochromous zonal wind, meridional temperature gradient and

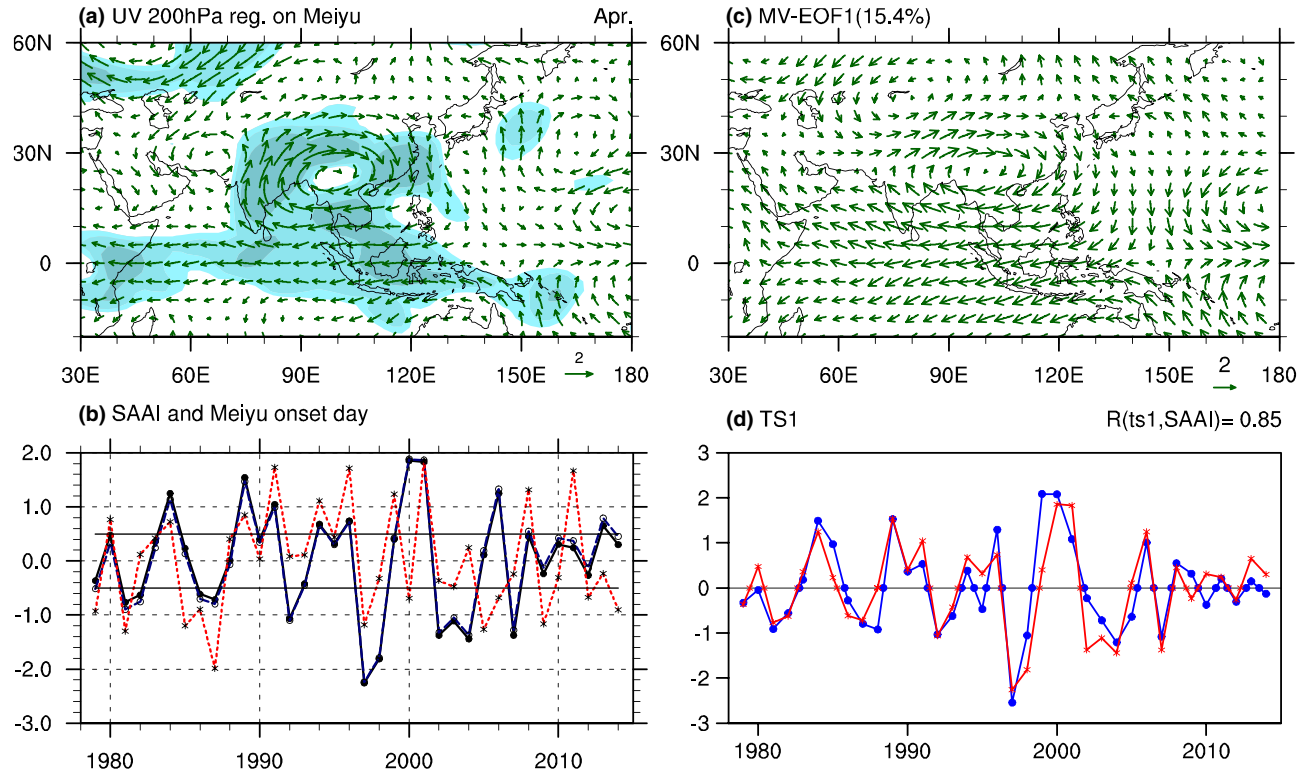

Fig. 1 **a** Regression wind fields at 200 hPa in April onto the Meiyu onset day, three-layer shaded areas ranging from light to dark denote the regions where the anomalies are statistically significant above the 90, 95 and 99% confidence levels using Student's *t* test. **b** The South Asian anticyclone index (SAAI) and the Meiyu onset day: solid (dashed) blue line delineates the detrended (raw) SAAI, and the red line delineates the detrended onset date index of the Meiyu. All the indexes are standardized. **c** Denotes the first leading mode of MV-EOF for 200-hPa meridional and zonal wind. **d** The time series of MV-EOF1 and SAAI

Table 1 The onset date of Meiyu in each year

Year	Data	Year	Data	Year	Data	Year	Data	Year	Data
1979	19 Jun	1987	28 Jun	1995	12 Jun	2003	20 Jun	2011	06 Jun
1980	06 Jun	1988	10 Jun	1996	02 Jun	2004	14 Jun	2012	22 Jun
1981	22 Jun	1989	08 Jun	1997	24 Jun	2005	26 Jun	2013	20 Jun
1982	12 Jun	1990	14 Jun	1998	18 Jun	2006	22 Jun	2014	25 Jun
1983	10 Jun	1991	02 Jun	1999	07 Jun	2007	19 Jun		
1984	07 Jun	1992	13 Jun	2000	20 Jun	2008	07 Jun		
1985	22 Jun	1993	14 Jun	2001	03 Jun	2009	26 Jun		
1986	20 Jun	1994	07 Jun	2002	19 Jun	2010	20 Jun		

atmospheric apparent heating [Q_1, calculated based on Yanai et al. (1973)] on the SAAI (Fig. 2, left panels) and SAHI (Fig. 2, right panels) were analyzed. The SAA-related significant positive and negative zonal wind anomalies are located in north of Tibet Plateau and Bay of Bengal respectively (Fig. 2a). The position is confined where the SAA is located (Fig. 1a, c). In addition, significant SAA-related positive and negative anomalous meridional temperature gradient is located in north and south of 20°N (Fig. 2b). It implies that the anomalous zonal wind can be explained by the anomalous meridional temperature gradient considering the thermal wind relationship. Meanwhile, anomalous atmospheric apparent heating sources related to the SAA over South Asia are significant (Fig. 2c), which change the local temperature and further the meridional temperature gradient above-mentioned that ultimately generates the SAA. By contrast, the SAH-related zonal wind, meridional temperature gradient, and Q_1 are less significant and located more eastward (Fig. 2d–f). It suggests different dynamic origin of the two climate systems.

The correlation coefficient between the SAAI and the Meiyu onset days is 0.48 (above the 99% confidence

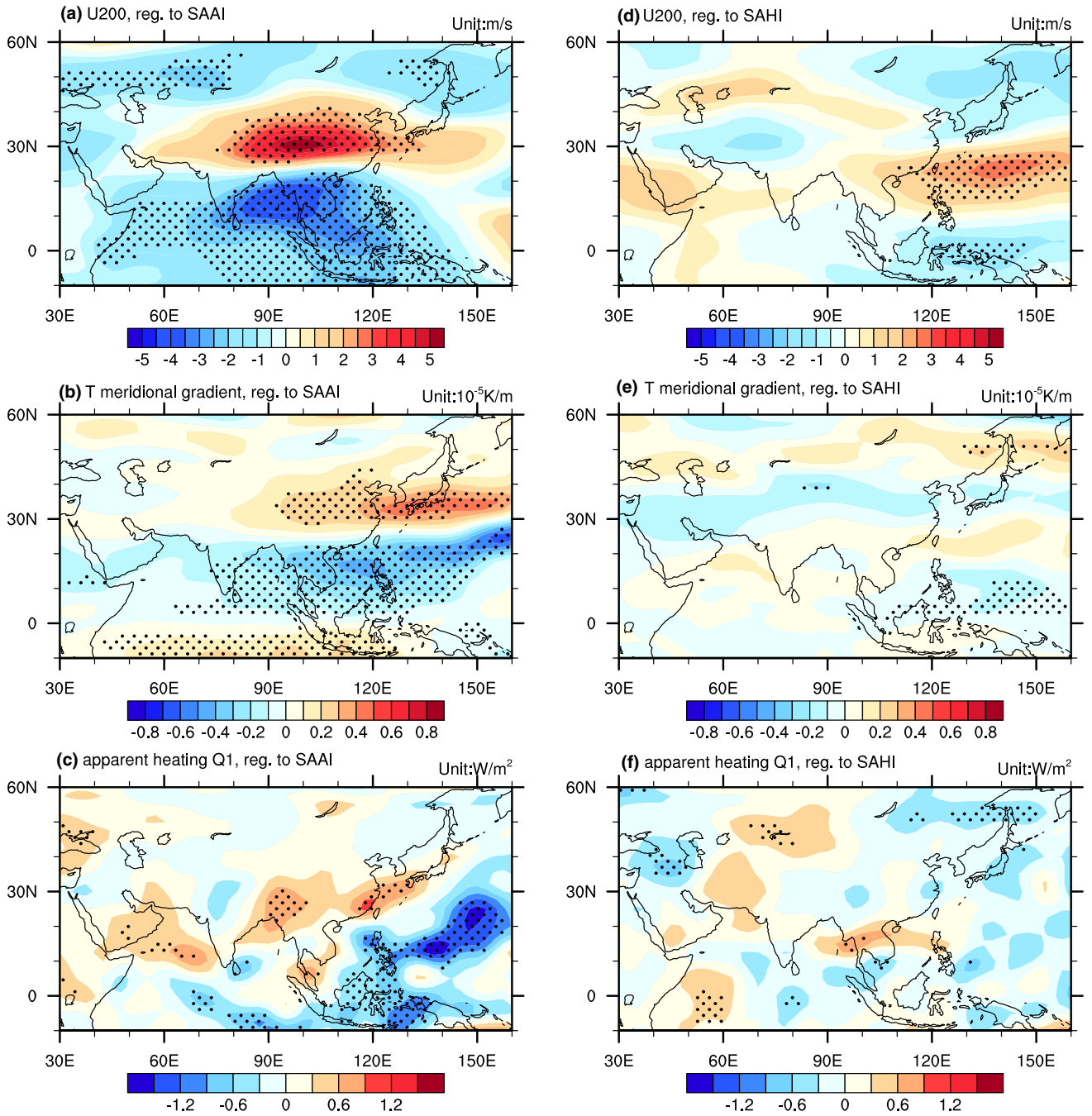

Fig. 2 **a–c** Respectively denote the regression map of zonal wind at 200 hPa, the average temperature meridional gradient on upper troposphere (300–200 hPa) and atmospheric apparent heating (Q_1) in April on SAAI. The dotted regions are statistically significant at the 95% confidence level, according to Student's *t* test. **d–f** As for **a–c** respectively, but for regression on SAHI

level estimated by Student's *t* test), and the results derived from the detrended and raw data show rare differences. The significant connection between the SAAI and the Meiyu onset days suggests that the variability of the April SAA may be a potential predictor for the Meiyu onset. To better illustrate the potential relationship between the Meiyu-onset-related atmospheric circulation and the April SAA, stronger SAA years (SAAI $\geq$ 0.5; 1984, 1989, 1991, 1994, 1996, 2000, 2001, 2006, and 2013) and weaker SAA years (SAAI ≤ -0.5; 1981, 1982, 1986, 1987, 1992, 1997, 1998, 2002, 2003, and 2007) were defined.

4 SAA-related circulations and its effect on the Meiyu onset

4.1 The differences in circulation during strong and weak SAA years

We, therefore, examined the evolution of atmospheric circulation and precipitation anomalies related to the SAA on a sub-seasonal time scale. Figure 3a shows the difference of wind fields at 850 hPa between the strong and weak years from 1 June to 15 June, which is a crucial time for the Meiyu because the different circulation patterns in this period determine whether the onset of the Meiyu is earlier or later. Corresponding to a stronger-than-normal SAA in April, an anomalous anticyclone was evident from 1 June to 15 June over the regions from southern China to the western North Pacific (5°−30°N), indicating a stronger southwesterly flow in the downstream YHRB. It has been revealed that the Meiyu is generated by a northern shift of the East Asian summer monsoon (EASM) (e.g., Tao and Chen 1987; Chang 2004), and the southwesterly flow is, therefore, an important meteorological condition for the onset of the Meiyu. As a result, following a stronger-than-normal SAA in April, more moisture is transported to the downstream YHRB, and southwest of Japan in early June, providing favorable conditions for the earlier onset of the Meiyu. In addition, an anomalous anticyclone emerged over the WNP at 500 hPa. It implies the advancing westward and northward shift of the WPSH, which also promoted the southern transport of moisture into the YHRB (not shown). In addition, at 200 hPa, a dominant anomalous anticyclone was located over the Meiyu regions, including the regions of Baiu in Japan and Changma in Korea. It suggests the presence of divergence anomaly in the upper troposphere over the Meiyu regions in early June following a stronger-than-normal SAA in April. Such a divergence anomaly in the upper troposphere acts as a "pump" and enhances the local ascending motion and convergence in the lower layer of the troposphere, which leads to stronger southwesterly flow. It is noteworthy that an anomalous easterly flow was evident in the subtropics between 10°N and 30°N (not shown), suggesting a weakened subtropical jet stream in association with a stronger SAA. This weakened jet increases the mixing of the cooler and warmer air and also favors the earlier onset of the Meiyu (Lu et al. 2001; Zhu et al. 2011).

To provide more details on the differences in atmospheric circulation related to the Meiyu onset process in strong and weak years of the SAAI, the characteristics of the anomalous circulations at 850 hPa and the WPSH were analyzed pentad by pentad. The first three pentads of June are illustrated in Fig. 3b–d, respectively. During 1 June to 5 June as well as 6 June to 10 June, the southwesterly flow over the south of China was apparently stronger associated with the stronger-than-normal April SAA (Fig. 3b, c). The evolution of the WPSH, indicated by the 5880 isoline, is shown in Fig. 3e pentad by pentad under different SAAI conditions. Compared with the situation associated with weaker-than-normal SAA in April (Fig. 3e; blue isoline), the WPSH following a stronger-than-normal SAA extended to the west of 120°E in early June, and the ridgeline moved over 20°−25°N (Fig. 3e; red isoline). Such an anomalous atmospheric circulation is favorable for the earlier onset of the Meiyu (Ding 1992; Ding et al. 2007).

4.2 The differences in precipitation between stronger and weaker SAA years

In the previous subsection, it was indicated that the atmospheric circulation anomalies in early June that are related to the stronger-than-normal April SAA are favorable for the earlier onset of the Meiyu. In this section, further details of the evolution of the precipitation are provided.

The emergence of the constant rain belt in the Meiyu region is regarded as the beginning of the rainy season in the YHRB. To illustrate the development of the rain belt, the evolutions of the rain belt (averaged in 110°E–122°E) in strong and weak SAA years are shown in Fig. 4a, b, respectively. In years of stronger SAA, the rain belt passed through the south boundary (28°N) of the Meiyu regions in the end of May and the maximum rain center moved into the Meiyu regions before 10 June (Fig. 4a). In contrast, maximum rain center moved into the Meiyu regions on around 20 June (Fig. 4b), when the April SAA was weaker than normal. To specifically detect the different transitions of the rain belt and their relationship with the horizontal wind, the time-latitude distributions of the differences in the OLR and 850 hPa winds (averaged over 110°–122°E) between strong and weak SAA years are shown in Fig. 4c. Apparently, the anomalous southwesterly wind began to prevail from 21 May; however, it was mainly confined to the region south of 20°N. The anomalous southerly wind moved northward at the end of May and moved into the Meiyu regions (north of 28°N) after 31 May. From 1 June to 10 June, a dominant southerly anomaly prevailed over the Meiyu regions (Fig. 4c: vectors). Those southwesterly winds were associated with the enhanced convection over the Meiyu regions in early June, especially with the most prominent convection from June 5 to June 10 (Fig. 4c: negative in shading). Notably, concurrent with the northward shift of the southerly anomaly, a northward propagation of negative OLR anomalies from south of China to the YHRB during 26 May to 10 June was also evident. Apparently, the time evolutions of the precipitation, low-level winds, and OLR over the Meiyu regions

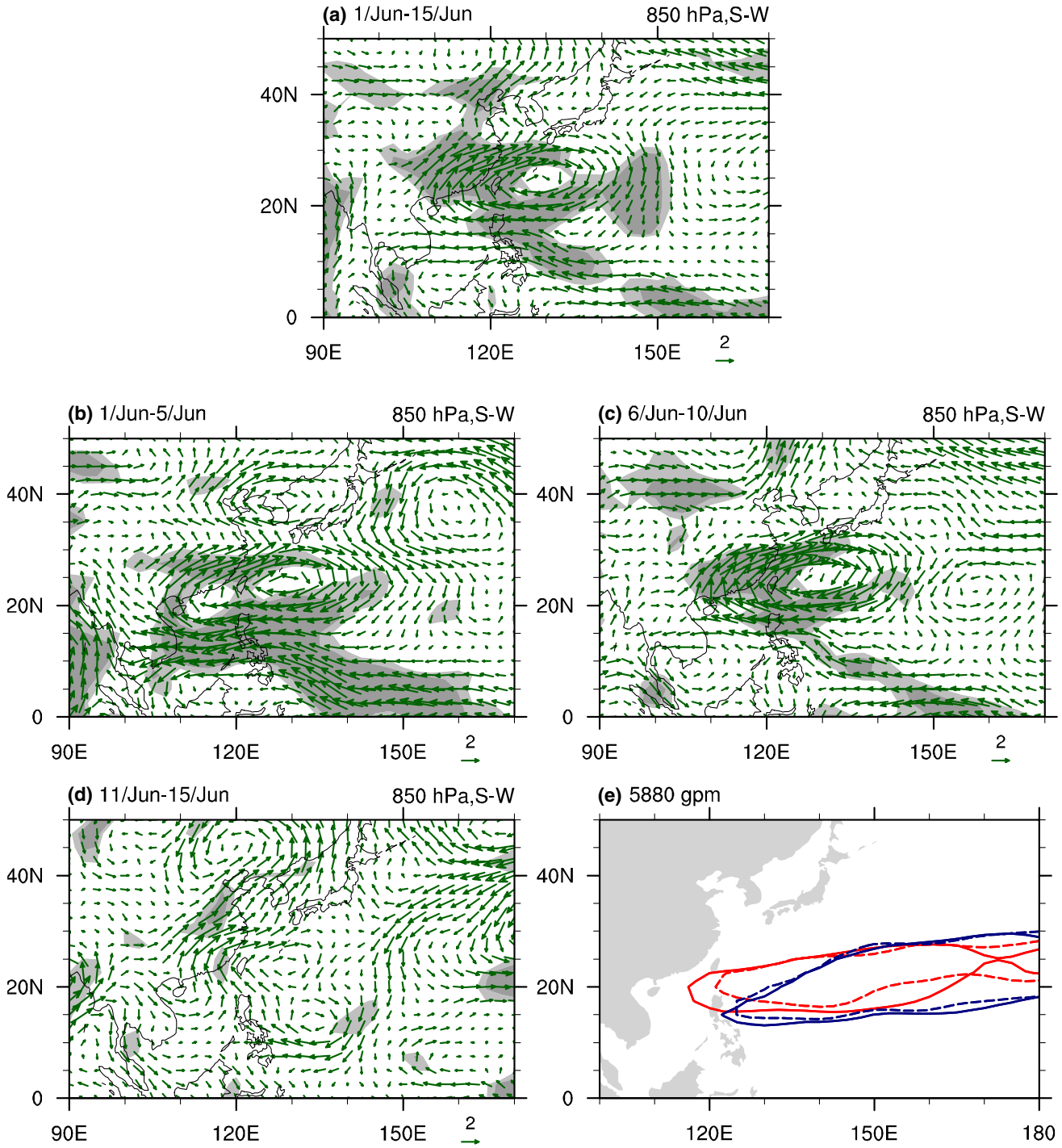

Fig. 3 **a** Difference wind fields at 850 hPa between strong years and weak years of the SAAI during 1 June to 15 June. **b**–**d** Same as for **a**, but for the first, second and third pentads in June, respectively. The light and dark shaded areas indicate the regions where the differences are statistically significant above the 90 and 95% confidence levels by Student's *t* test, respectively. **e** 5880 gpm isoline in stronger/weaker SAA years (red/blue); the solid (dashed) lines are for 6 June–10 June (1 June–5 June)

indicate that the onset of the Meiyu would be earlier than normal when the April SAA is stronger than normal.

To further examine the evolutions of the precipitation anomalies concurrent with the evolution of atmospheric anomalies that are associated with the April SAA (Fig. 4), the spatial distributions of the precipitation difference between stronger and weaker SAA years were analyzed pentad by pentad (Fig. 5). Compared with the precipitation

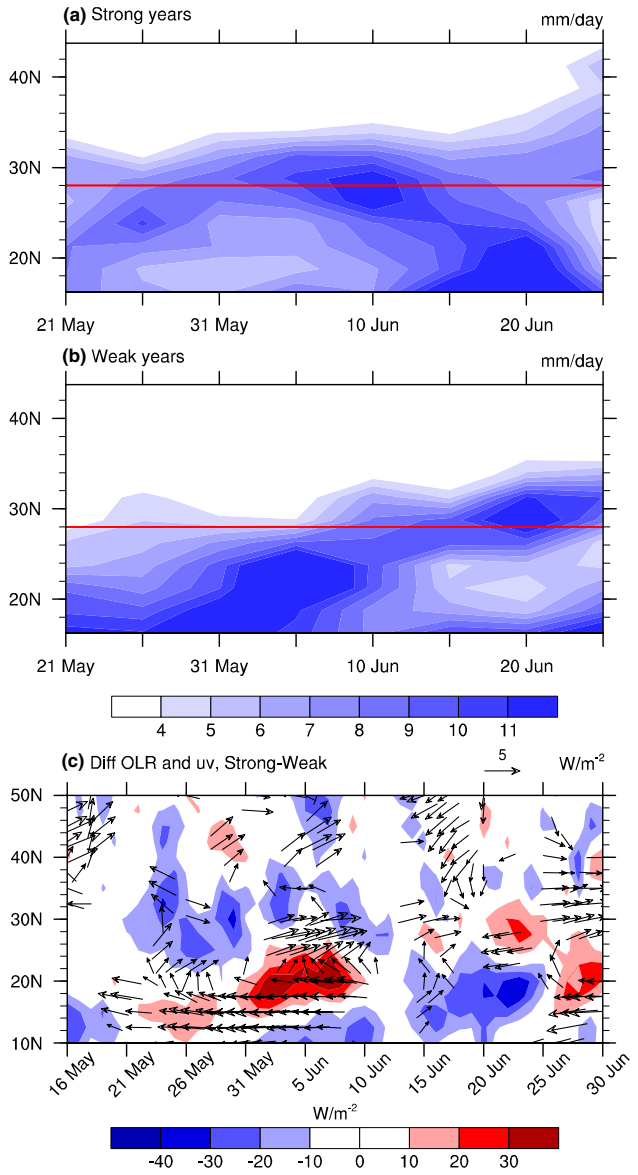

Fig. 4 Time–latitude plot of precipitation averaged along 110°E–122°E in **a** the strong years and **b** the weak years of the SAAI. The red reference line denotes the southern boundary of the Meiyu regions (28°N). **c** The time-latitude diagram of OLR and 850 hPa wind field differences between the strong years and weak years of the SAAI averaged along 110°E–122°E. The arrows indicate wind field differences that are significant at a 90% level using Student's *t* test, and the shading shows the OLR differences

associated with the weaker-than-normal April SAA, the precipitation was more abundant over the Meiyu region from 31 May to 5 June (Fig. 5a). From 5 June to 10 June, the precipitation over the Meiyu regions intensified dramatically (Fig. 5b), indicating the earlier onset of the Meiyu. Interestingly, a tripole rainfall anomaly pattern with northwest–southeast direction was observed when the Meiyu was established (Fig. 5b), with three precipitation anomaly centers located in the Meiyu regions, the WNP between 15°N and 25°N and the Philippine Sea (PHS) from north to south. The north–south oriented tripole rain pattern was well consistent with the distribution of the OLR from 31 May to 10 June (Fig. 4c: shading; the negative, positive, and negative anomalies located approximately 10°N, 20°N, and 30°N), suggesting significant anomalous ascending, descending, and ascending motions from south to north. Those vertical motions, which were associated with the tripole rainfall pattern, may have constituted meridional overturning circulation (Nitta and Hu 1996, Hsu and Lin 2007), which in turn might have played a crucial role in the excitation and maintenance of the tripole rainfall pattern. It should be noted that the convection over the PHS (approximately 10°N, Fig. 4c: shaded) is critical in exciting a northward wave train (Nitta and Hu 1996), implying a potential teleconnection between the PHS precipitation and the Meiyu, which will be further explored in the next section. Due to the establishment of the Meiyu after 11 June in both the stronger and weaker SAA years, the precipitation showed rarely differences (Fig. 5c).

5 Possible mechanisms linking the SAA in April with the onset date of the Meiyu

In the above section, we described the connection between the SAAI and the onset date of the Meiyu. In this section, the possible physical mechanisms will be addressed.

We first examine the evolution of the SAA-related circulation from April to June pentad by pentad, as illustrated in Fig. 6. It is evident that an anomalous anticyclone over South Asia persisted from April to early May (Fig. 6a–g), which gradually began to move eastward from 26 April and dissipated on approximately 16 May. As the SAA shifted eastward, a significant anomalous anticyclone emerged over the WNP from 26 April to 15 May (Fig. 6f–i). The anomalous anticyclone in the upper troposphere corresponded to the anomalous divergence and favored an anomalous ascending motion, indicating that the eastward shift in the SAA might change the atmospheric circulation in the lower troposphere. Another notable feature was the meridionally oriented distribution of the anomalous cyclone and anticyclone over the PHS and WNP from 26 April to 15 May (Fig. 6f–i), implying the potential existence of a meridional wave train or teleconnection pattern along 140°E. Therefore, the evolution of the SAA suggests that the anomalous SAA persisted from 1 April to 15 May in the upper troposphere (at approximately 200 hPa) and shifted eastward gradually. Subsequently, it changed the lower level atmospheric circulation through the pumping effect or by establishing a meridional overturning wave pattern.

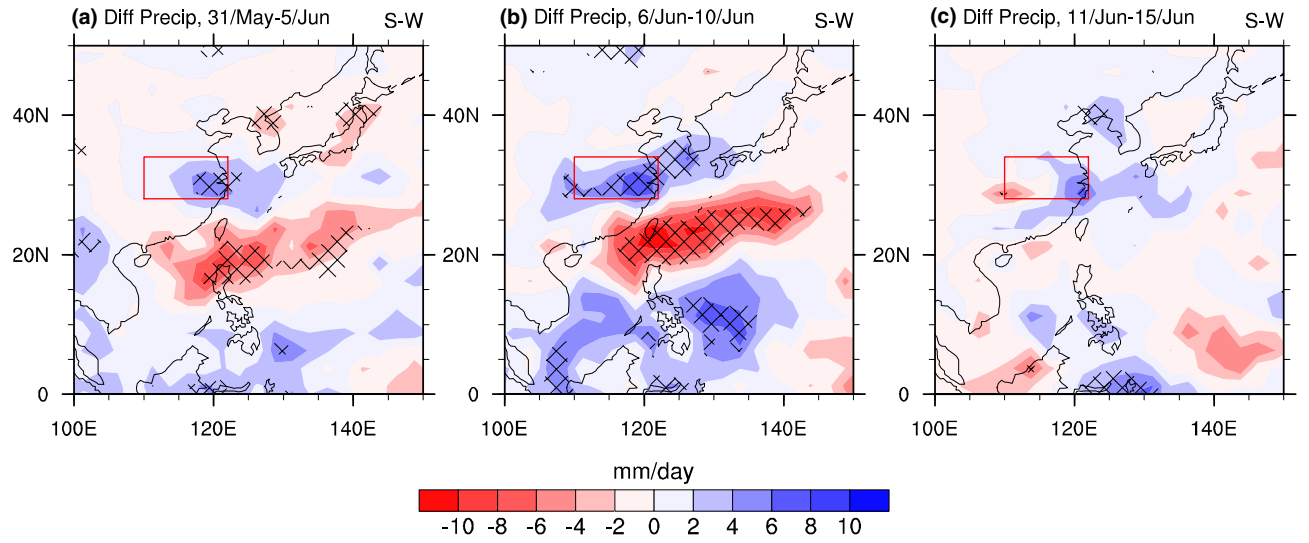

Fig. 5 Differences in precipitation between the strong and weak years of the SAAI during **a** 31 May to 5 June, **b** 6 June to June 10, and **c** 11 June to June 15. The red frame bounds the Meiyu regions of China, and the gridded areas indicate where the differences are significant at the 95% confidence level using Student's *t* test

Prior to analyzing the effect of eastward shifting of the SAA, the possible reason for the eastward shifting should be addressed. As illustrated by Fig. 2a, the SAA is generated directly by the increasing and decreasing of the westerly in north and south of 25°N over the South Asia. Thus, the evolution of zonal wind difference in north and south around 25°N between strong and weak SAAI years was analyzed (Fig. 7a). The distribution of significant anomalous zonal wind in north and south is similar but with the opposite signs, the significant anomalies are persistent during April around 90°E. Interestingly, the significant anomalies moved to east in late April, consistent with the above analysis (Fig. 6). Meanwhile, apparent enhanced and weakened meridional temperature gradient were located in the north and south, which also shifts eastward in late April (Fig. 7b). The evolutions of both zonal wind and meridional temperature gradient anomalies accorded with the thermal wind relationship. Thus, the eastward-moving SAA was driven by the eastward-moving meridional temperature gradient, which may be induced by seasonality. The temperature difference between strong and weak of SAA averaged along 20°−30°N, which is located in the middle of increased and decreased zonal wind regions, is shown in Fig. 7c to address the mechanism. The spatial distributions of significant temperature anomalies are similar with zonal wind and meridional temperature gradient anomalies, which also move to east in late April. To explain the meridional temperature gradient anomalies, the zonal energy transport [u^*E; Graversen and Burtu (2016)] is analyzed; here, u is zonal wind, and E ($=c_pT + gz + Lq$) is the energy (Ou et al. 1989); where c_p is the specific heat capacity at constant pressure and T is air temperature, g is the gravitational acceleration, z is the height, L is the latent heat of condensation, and q is specific humidity. Given that the uc_pT is dominant in the zonal energy transport, thus we only show the results of uc_pT. It is apparent that zonal energy transport anomaly is prominent in late April to early May (Fig. 7d). Thus, the maximum value of significant zonal energy transport over 135°E may heat the atmosphere and further increase the temperature over this region, resulting in increased and decreased meridional temperature gradient in the north and south of this region, and finally favoring the eastward-moving SAA.

To provide more details regarding the effects of the SAA's evolution, the change in vertical motion from the end of April to the end of May associated with the evolution of the SAA was further analyzed. Figure 8 shows the vertical–horizontal cross section of the vertical wind difference averaged along 115°E–145°E between the strong and weak SAA years from 26 April to 31 May. In the beginning stage of the eastward moving of the SAA, an apparent meridional overturning appeared over lower latitudes (0°–30°N), with a significant anomalous ascending motion located at 15°N–30°N as well as a significant anomalous descending motion located at approximately 10°N (Fig. 8a). Meanwhile, a dominant anomalous ascending motion emerged in the south tropics (20°S–0°), which may reinforce the tropical precipitation which began in early April (Fig. 9b). During that period, a rudiment of the meridional overturning pattern was established. As the tropical rain belt moved southward to the Philippine Sea from 1 May to 15 May (Fig. 9b), an apparent meridional overturning circulation, which resembled the PJ pattern (Hsu and Lin 2007) and might have been stimulated by the anomalous convection (Huang 1992), exhibited a quasi-barotropic and well-organized structure (Fig. 8d).

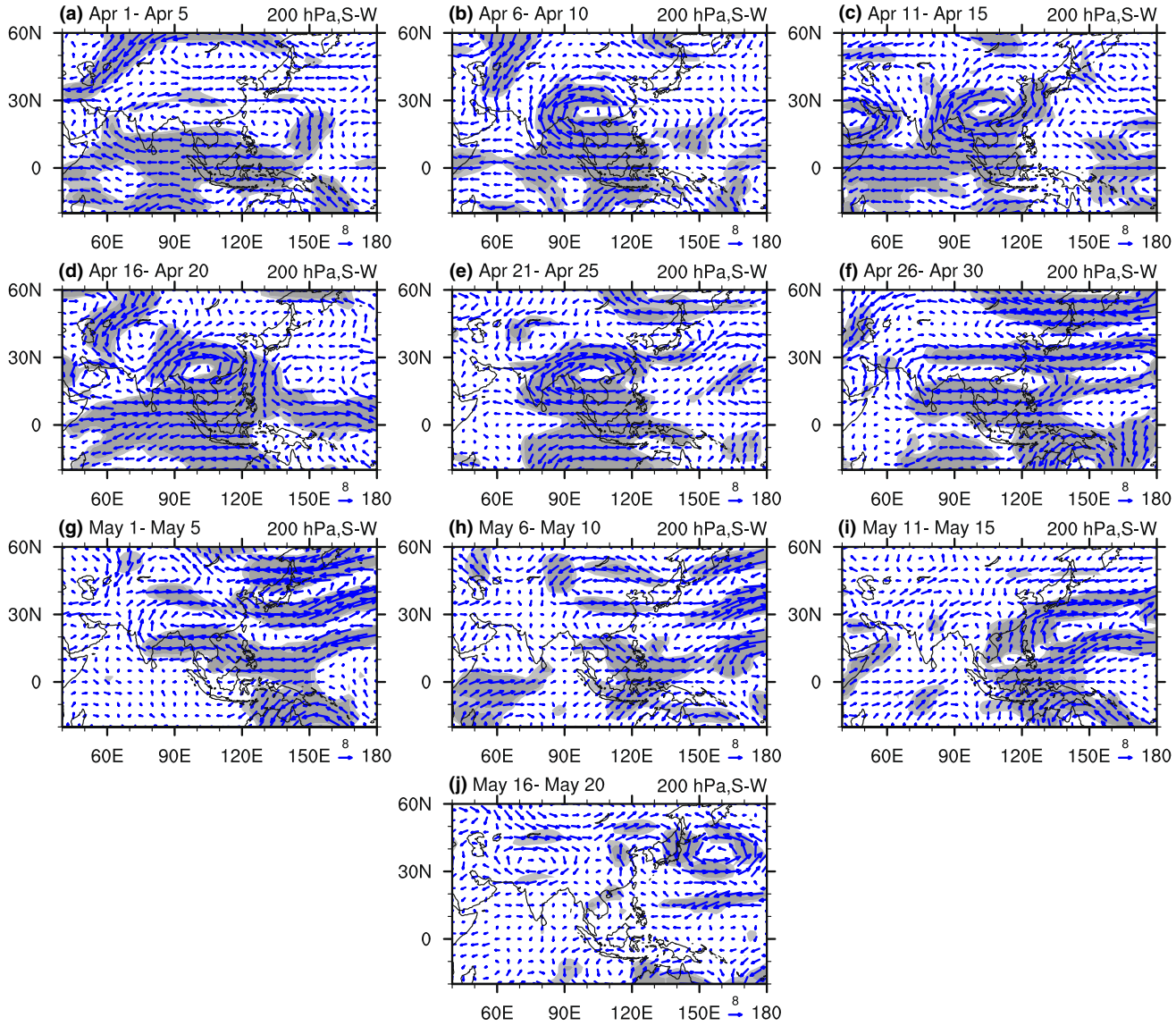

Fig. 6 The differences in the wind fields at 200 hPa between the strong and weak years of the SAAI from 1 April to 20 May pentad by pentad. The light and dark shaded areas indicate the regions where the differences are statistically significant above the 90 and 95% confidence levels using Student's *t* test, respectively

This is more evident from an inspection of the precipitation anomalies from 1 May to 15 May, which displayed negative, positive, and negative anomalies at approximately 5°N, 15°N, and 30°N, respectively (Fig. 9b). Such PJ-like pattern provides the fundamentals for the earlier onset of the Meiyu.

The above analysis indicates that the moving-southward ascending motion before 21 May plays a crucial role in establishing the PJ-like pattern. Furthermore, we also examined the factors causing this southward moving. It is revealed that the WPSH influences greatly the East Asia climate (e.g., Lu 2001; Mao et al. 2010; Huang et al. 2014; Huang and Li 2015; Huangfu et al. 2015). In addition, the ascending motion during the beginning stage of the eastward motion of the SAA occurs at the location of climatological WPSH. Lu (2001) suggested that the level of 925 hPa is better than 850 hPa for a vorticity analysis of the WPSH. Therefore, in this paper, we employed the vorticity at 925 hPa to examine the interaction between the WPSH and the anomalous ascending motion (Fig. 9a). The time-latitude diagram of vertical motion (the first plot in Fig. 9a) suggests the notable moving-southward ascending motion from late April to late May. Meanwhile, the vorticity at 925 hPa between strong and weak SAA years shows the positive difference (the second plot in Fig. 9a), implying that the anomalous ascending motion reduces the pressure at low level and further decreases the intensity of WPSH. These results imply

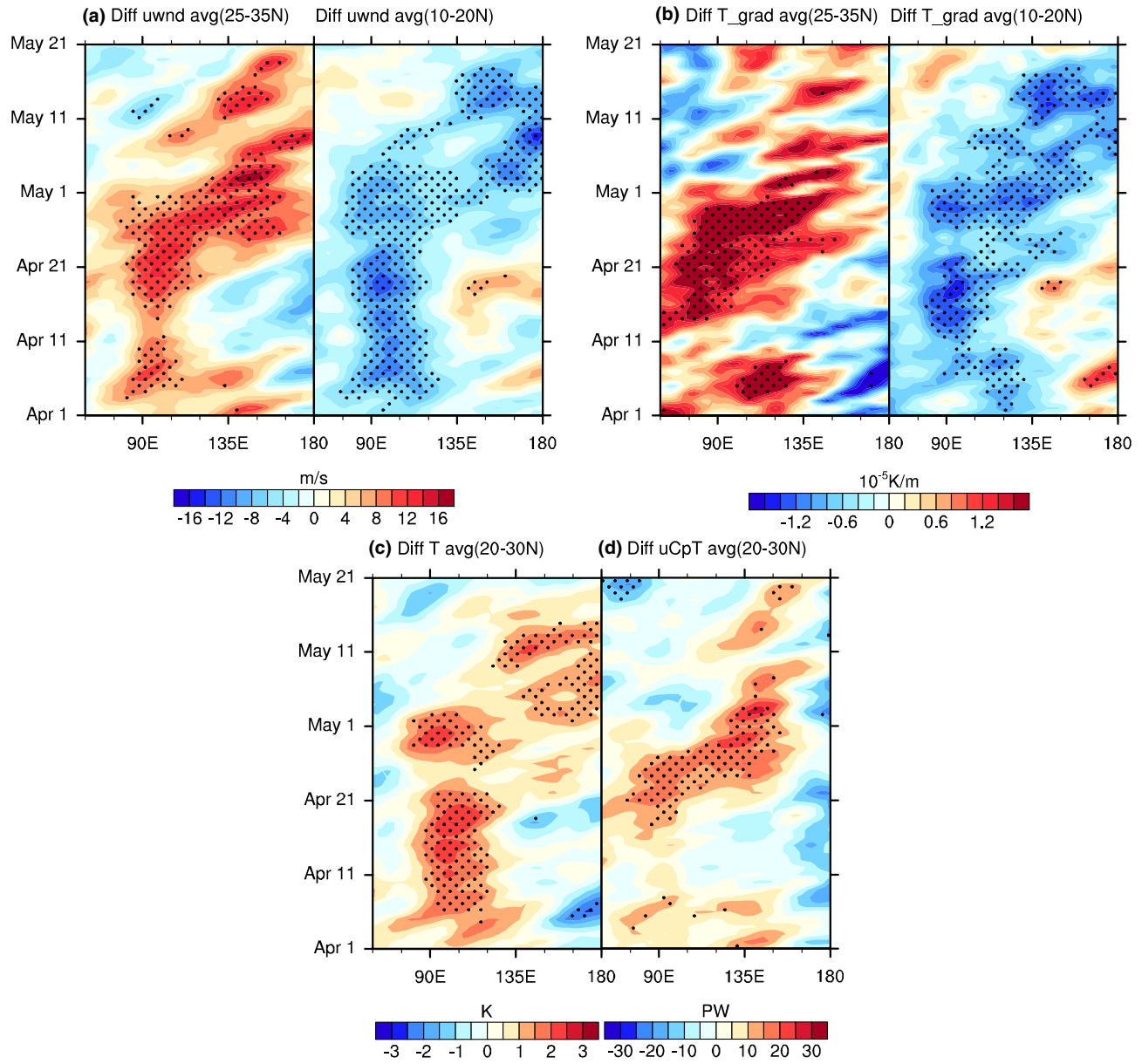

Fig. 7 **a** The time-longitude diagram of zonal wind difference (the left demonstrate the average along 25°−35°N and the right is average along 10°−20°N) between strong and weak years of SAAI. **b** As in **a** but for the meridional temperature gradient in the upper troposphere (300–200 hPa). **c** The temperature difference averaged along 20°−30°N in the upper troposphere (300–200 hPa). **d** as in **c** but for zonal energy transport. The dotted regions are statistically significant at the 95% confidence level, according to Student's *t* test

that the interaction between WPSH and ascending motion may affect the moving-southward ascending motion.

On the other hand, the large-scale latent heat associated with abnormal precipitation might promote the earlier northward shift of the WPSH (e.g., Liu et al. 2001; Wen and Shi 2006; Lu 2001). As illustrated in Fig. 3e, in years of strong SAA, the northward shift of the WPSH occurs earlier than normal, with a ridgeline position approximately 20°–25°N, and the western points of the WPSH are found in the west of 120°E. The relationship of the heating source with the intensity and position of the WPSH has been studied extensively (e.g., Liu et al. 2001; Lu and Dong 2001; Lu 2001; Feng et al. 2017). Wen and Shi (2006) showed that the position of condensation heating plays an important role in the shape and position of the WPSH. When condensation heat energy is released on the south side of the WPSH, the effect of the heating promotes the northward shift of the WPSH. To examine the effect of the heating source associated with the evolution of the SAA, we calculated the different integrated atmospheric apparent heat sources (Q_1) between the

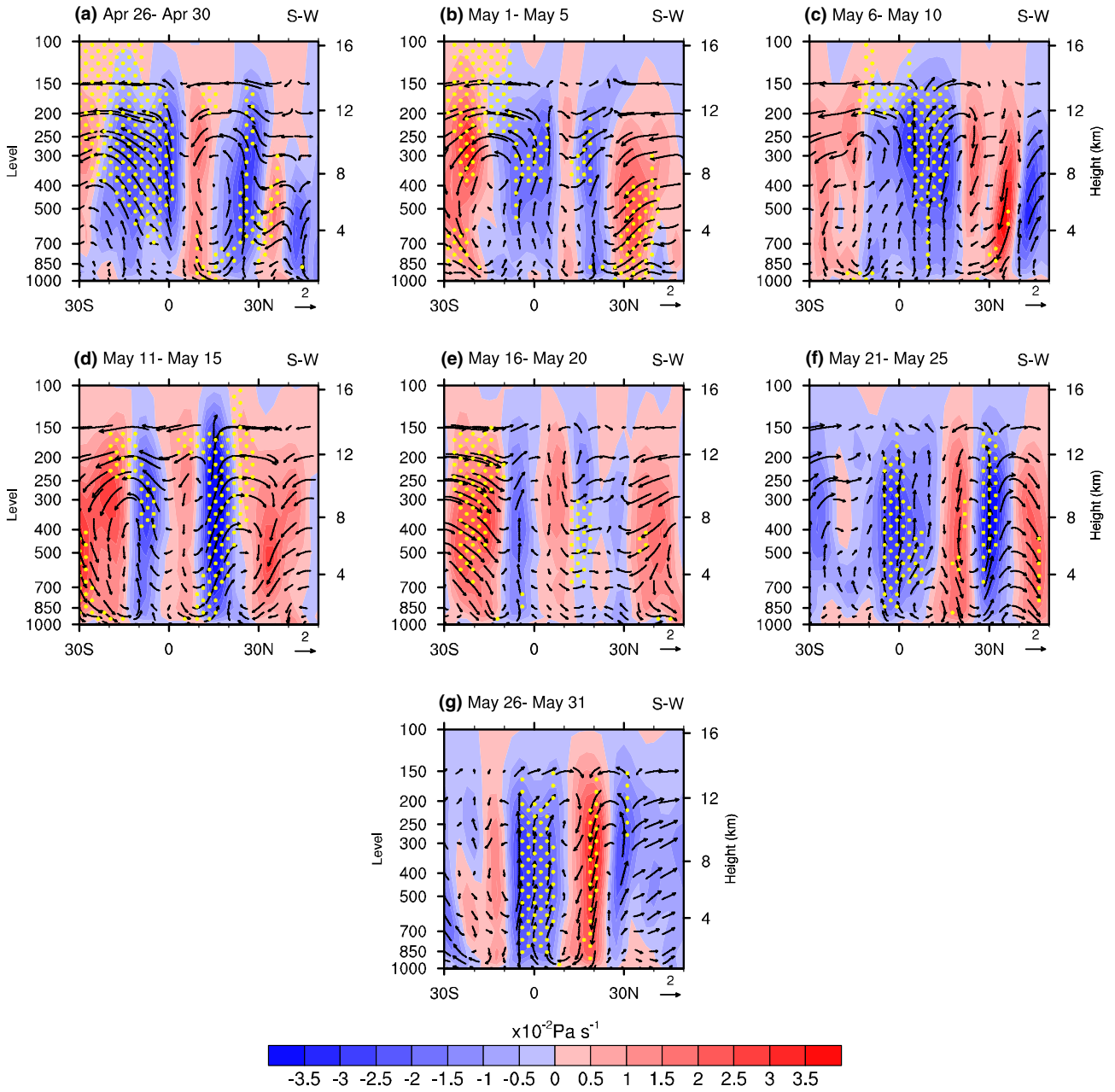

Fig. 8 Vertical–horizontal cross section (averaged along 115°–145°E) for the vertical wind (vectors) and omega (shading) difference fields between the strong and weak years of the SAAI from 26 April to 31 May pentad by pentad. The differences in the dotted regions are statistically significant at the 90% confidence level, according to Student's *t* test

strong and weak SAAI years over the region (5°S–15°N, 120°E–140°E). It is apparent that the Q_1 difference was almost completely positive from April to June (Fig. 9c). Interestingly, a dominant increasing in integrated atmospheric Q_1 appeared on 21 May, which corresponds well to the abrupt and positive rainfall anomalies over the PHS (Fig. 9b). Such prominent positive integrated atmospheric Q_1 on the south side of the WPSH can promote the northward shift of the WPSH. The differences of the integrated atmospheric Q_1 between the strong and weak SAA years displayed negative anomalies over the regions (15°N–30°N, 120°E–140°E) (not shown). Such a strong meridional contrast in heating could also favor the northward shift of the WPSH (Cao et al. 2002).

To further examine the evolution of the WPSH, the different circulations at a lower level (850 hPa) between the strong and weak SAA years are displayed pentad by pentad from 1 April to 30 June (Fig. 10). Corresponding to the anomalous

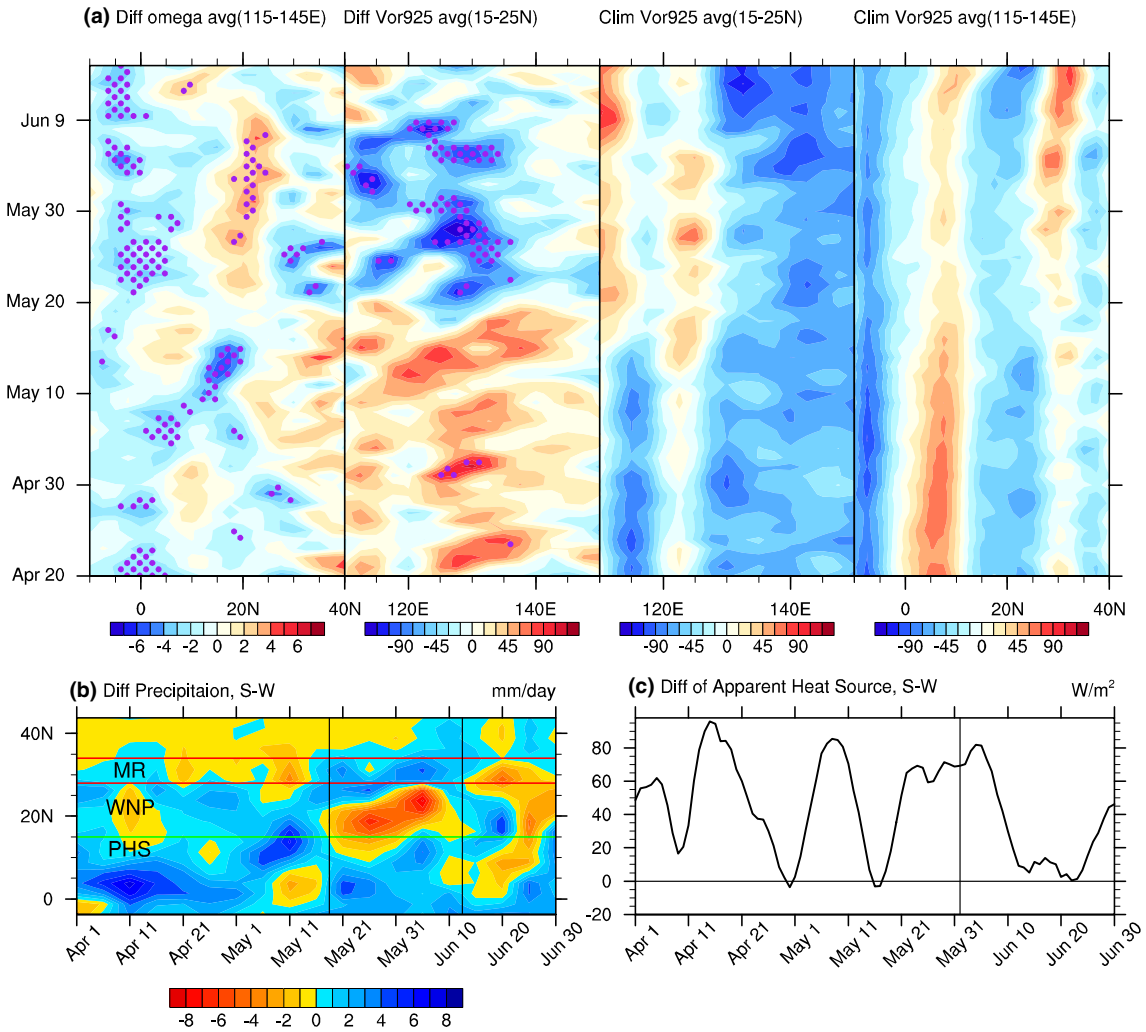

Fig. 9 **a** the first plot denotes the different omega averaged from middle to upper troposphere (500–200 hPa, unit is 0.01 Pa s^{-1}) between strong and weak years of SAAI. The second plot denotes the vorticity difference averaged along 15–25°N at 925 hPa (units is 10^6 s^{-1}). The dotted regions indicate the difference statistically significant at the 90% confidence level, according to Student's *t* test. The third and fourth plots denote the climatological mean of the vorticity averaged along 15°−25°N and 115°−145°E at 950 hPa, respectively. **b** The diagram of the temporal evolution of precipitation difference between the strong and weak years of the SAAI during April to June. MR denotes the Meiyu region (28°−34°N, 110°−122°E), PHS denotes the Philippine Sea (5°S–15°N, 120°−140°E), and WNP denotes the western North Pacific. **c** Denotes the regionally averaged (5°S–15°N, 120°E–140°E) differences of the integrated atmospheric apparent heat sources for the strong and weak years of the SAAI

anticyclone at the upper level from 21 April to 5 May due to the eastward shift of the SAA (Fig. 6e–g), the most dominant feature at the lower level was the anomalous cyclone in the WNP, which began to appear on 21 April and persisted to 5 May (Fig. 10e–g). Such a configuration, with an anomalous anticyclone at the upper level and anomalous cyclone at the lower level, is attributable to the dominant anomalous vertical motions (Fig. 8a–d). The gradual anomalous cyclone shifted to the south after 5 May (Fig. 10h) and moved into the PHS from 11 May and 15 May (Fig. 10i). The southward shift of the anomalous cyclone coincided well with the abrupt increase in rainfall over the PHS (Fig. 9b). Abundant precipitation over the PHS can induce large amounts of latent heat, which might promote the earlier northward shift of the WPSH (Cao et al. 2002). As shown in Fig. 10k, an anomalous anticyclone emerged in the WNP during 21–25 May, indicating the intensification of the WPSH. It was further supported by the dominant negative precipitation anomalies between 12.5°N–22.5°N subsequent to 21 May (Fig. 9b). As a consequence, the rainy season over the YHRB built up in the end of May, which, however, could not be referred to as the Meiyu because the position of the WPSH ridge was still located south of 20°N. Subsequently, the anomalous anticyclone strengthened and moved westward and northward from 26 May to 10 June (Fig. 10l–n). The northward extension of negative precipitation between

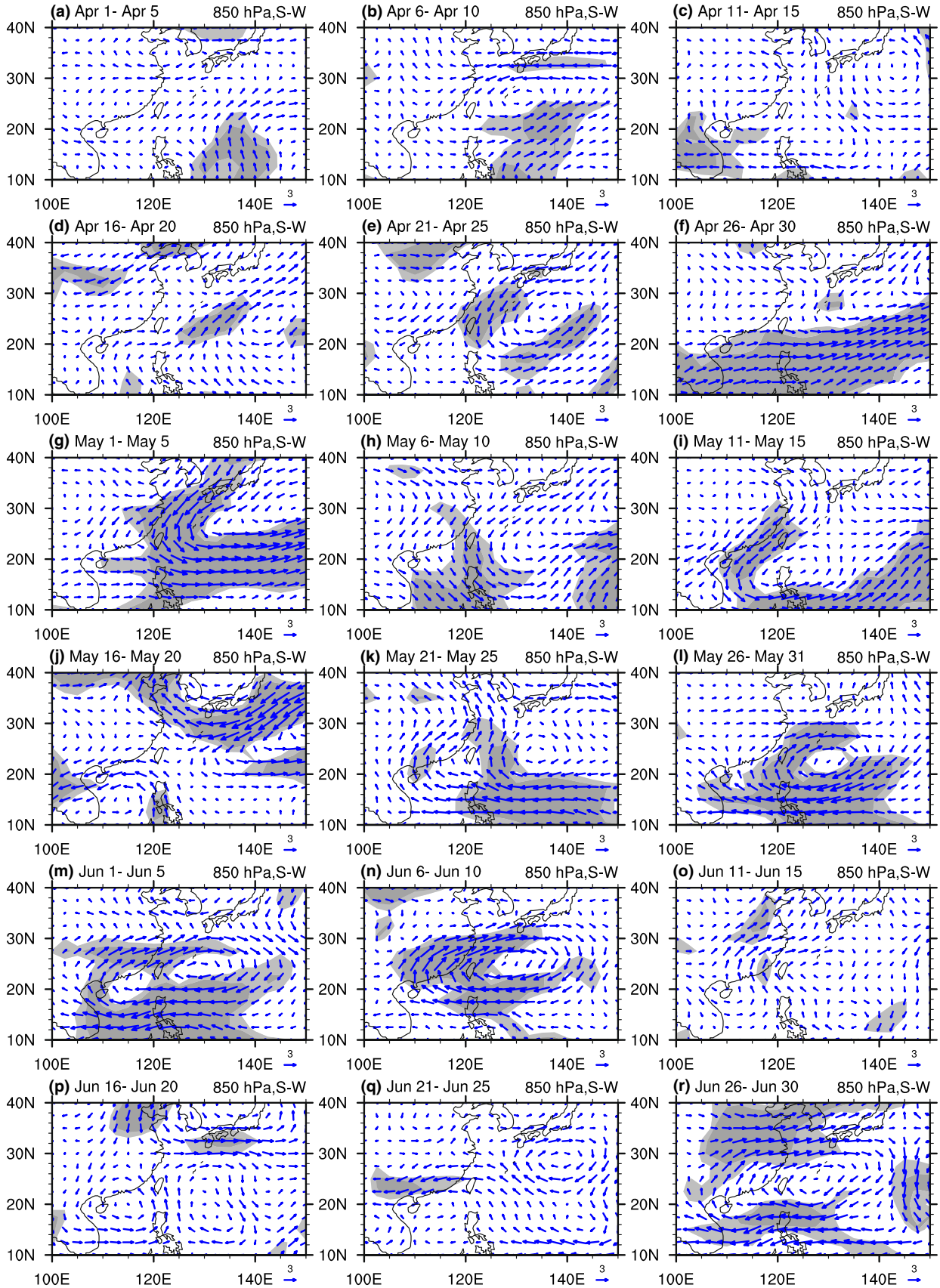
(a) Apr 1- Apr 5 850 hPa,S-W
(b) Apr 6- Apr 10 850 hPa,S-W
(c) Apr 11- Apr 15 850 hPa,S-W
(d) Apr 16- Apr 20 850 hPa,S-W
(e) Apr 21- Apr 25 850 hPa,S-W
(f) Apr 26- Apr 30 850 hPa,S-W
(g) May 1- May 5 850 hPa,S-W
(h) May 6- May 10 850 hPa,S-W
(i) May 11- May 15 850 hPa,S-W
(j) May 16- May 20 850 hPa,S-W
(k) May 21- May 25 850 hPa,S-W
(l) May 26- May 31 850 hPa,S-W
(m) Jun 1- Jun 5 850 hPa,S-W
(n) Jun 6- Jun 10 850 hPa,S-W
(o) Jun 11- Jun 15 850 hPa,S-W
(p) Jun 16- Jun 20 850 hPa,S-W
(q) Jun 21- Jun 25 850 hPa,S-W
(r) Jun 26- Jun 30 850 hPa,S-W
40N
30N
20N
10N
100E
120E
140E
3

◂**Fig. 10** The difference wind fields at 850 hPa between the strong and weak years of the SAAI from 1 April to 30 June pentad by pentad. The light and dark shaded areas indicate the regions where the differences are statistically significant at the 90 and 95% confidence levels using Student's *t* test, respectively

15°N and 27.5°N from 21 May to 10 June (Fig. 10b) confirmed the northward shift of the WPSH. As a result, the anomalous southwesterly wind began to prevail over South China and moved northwestward (Fig. 10k–n), promoting the earlier onset of the Meiyu (Fig. 9b: positive rainfall anomaly at approximately 30°N).

In addition, the establishment of a PJ-like pattern after 21 May (Figs. 8d, 9b) may also have played an essential role in the meridional position of the WPSH. Several previous studies have found that the PJ pattern is closely connected to the WPSH (Dai et al. 2002; Wang and He 2015). Moreover, Kurihara and Tsuyuki (1987) suggested that the atmospheric convection activities over the PHS could excite a northward-propagating Rossby wave, which is similar to the PJ pattern. Thus, the impact of the PJ-like pattern on the WPSH is also addressed. We employed the zonal wind at 850 hPa average along 110°−150°E to demonstrate the meridional position of the WPSH. The position of the WPSH ridge is denoted by the location of zonal wind equal to zero (Liu et al. 2012). The zonal wind difference between strong and weak SAA years and the corresponding 0 m s^{-1} isoline are given in Fig. 11. On the north and south sides of the ridgeline (0 m s^{-1} isoline in zonal wind) of WPSH prevail opposite sign zonal wind anomalies, respectively. After the PJ-like pattern established (around 21 May), significant anomalous easterly flow became prevailing at the low latitudes, suggesting the intensified and northward shift of the WPSH in strong SAI years. This feature is confirmed by the more northward location of 0 m s^{-1} isoline (the ridgeline of WPSH) in strong SAA years (solid line) than that in weak SAA years (dashed line).

6 Discussion and conclusions

In this study, we investigated the relationship between the SAA in April and the onset date of the Meiyu, as well as the related physical mechanisms. A schematic diagram regarding the observational findings and possible physical mechanisms is shown in Fig. 12.

We first used the definition of Ding et al. (2007) to calculate the Meiyu onset dates from 1979 to 2014, and the time series of the Meiyu onset dates showed large interannual variability. Based on the regressed atmospheric circulation maps at the lead times of the Meiyu onset, we found that the anticyclone in the upper troposphere over South Asia in April had the most significant relationship with the Meiyu onset dates. Meanwhile, the first leading mode revealed by MV-EOF analysis on the upper tropospheric zonal and meridional wind in April is similar with SAA related to the Meiyu onset dates, suggesting that the SAA is a robust climate system. Furtherly, we also examine the dynamic origin of SAA, and the results showed that the atmospheric apparent heating sources over the South Asia was responsible for the formation of the SAA. Subsequently, the SAA was introduced as a precursory climate system associated with the onset of the Meiyu. The results indicated that the significant relationship between the SAA in April and the onset date of the Meiyu is not only a statistical connection but also a physical teleconnection. Generally, stronger SAA in April is followed by earlier onset dates of the Meiyu, and vice versa.

The SAA emerges in early April and then moves eastward to the western North Pacific (WNP) in the late pentad of April. It is revealed that the abrupt significant zonal energy transport in the late April is responsible for the moving-eastward SAA. The eastwards SAA causes anomalous divergence in the upper troposphere and anomalous convergence in the lower layer over the WNP, which results in a meridional overturning circulation. Meanwhile, the divergence anomaly induces anomalous ascending motion in situ due to Ekman pumping, leading to an anomalous cyclone in the lower levels over this region. Due to the southward-moving ascending motion and lower tropospheric cyclone in the fourth pentad of May, the precipitation moves southward to the PHS. The interaction between ascending motion and WPSH may directly be responsible for the southward-moving ascending motion and lower tropospheric cyclone. The associated stronger convection over the PHS further reinforces the meridional overturning pattern, which develops into the PJ-like pattern and directly causes the tripole rainfall pattern (on approximately 21 May). The PJ-like pattern persists from the end of May to the beginning of June and facilitates the earlier onset of the Meiyu.

On the other hand, due to the increased heating resulting from the precipitation anomaly in the PHS from 21 May, the meridional temperature gradient is enhanced, promoting the earlier northward shift of the WPSH. In addition, the PJ-like pattern also plays an important role in the meridional displacement of the WPSH. The location of the WPSH provided the requisite large-scale circulation adjustment for the beginning of the Meiyu. Ultimately, the establishment and maintenance of the PJ-like pattern as well as the earlier northward shift of the WPSH cause stronger-than-normal southwesterly flows and additional water vapor transport to the YHRB, leading to an earlier start of the Meiyu. These results have enhanced our understanding of the relationship between the April SAA and onset date of the Meiyu. Thus, it is concluded that in stronger (weaker) SAA years, southwesterly airflow is stronger (weaker) than normal. As a result, the northward shift of the monsoon rain belt occurs

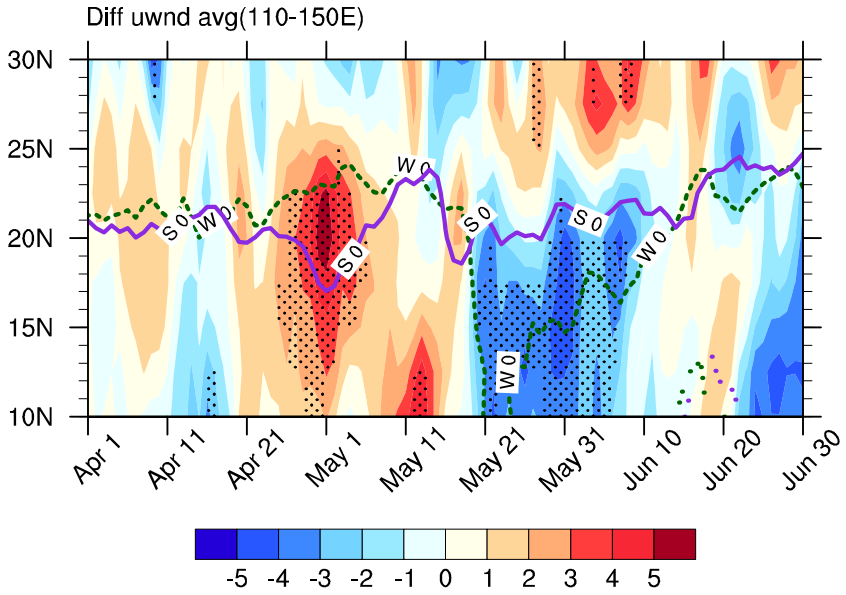

Fig. 11 Different zonal wind averaged along 110°−150°E between strong and weak SAAI years. The dotted regions indicate the differences statistically significant at the 90% confidence level, according to Student's *t* test. The solid (with the label "S 0") and dash (with the label "W 0") lines denote the 0 m s^{-1} location to demonstrate the WPSH meridional position in strong and weak SAAI years, respectively

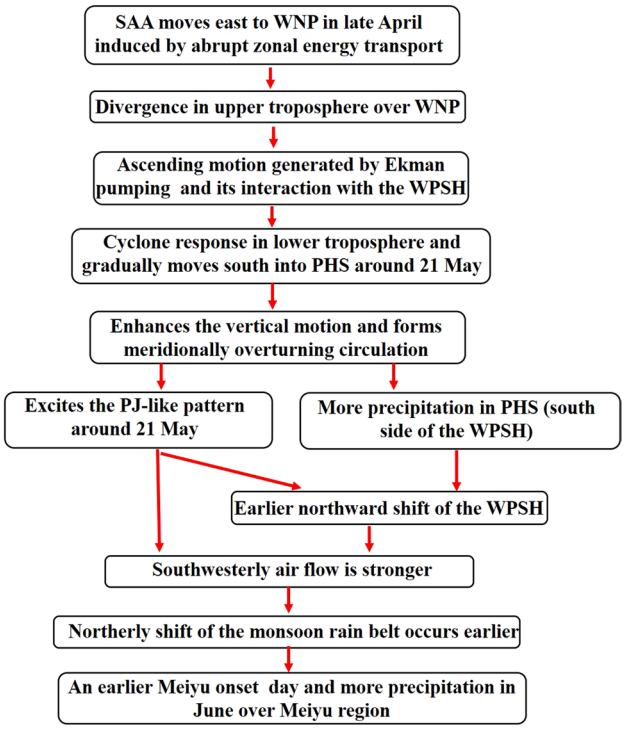

Fig. 12 A schematic diagram of the possible physical processes that the SAA imparts on the Meiyu in strong years of the SAAI

earlier (later), which favors an advanced (delayed) onset of the Meiyu and more (less) precipitation in June over the Meiyu region.

Previous studies have documented that the beginning of the Meiyu is strongly influenced by the tropical synoptic system and is also modulated by the atmospheric circulation patterns that occur simultaneously at the mid- and high-latitudes (Tao and Chen 1987; Huang et al. 2011; Li and Zhang 2014). This study addresses the preceding atmospheric circulation patterns and revealed a new and statistically significant relationship between the onset dates of the Meiyu and the April SAA, thus shedding light on the prediction of the Meiyu onset. It should be noted that the SAA can explain about 25% variance of the Meiyu onset dates. It means that there are other factors influencing the onset of Meiyu, which needs further investigation.

Acknowledgements This research was supported by the National Key Research and Development Program of China (Grant 2016YFA0600703), the National Natural Science Foundation of China (Grants 41605059, 41505073), and the Young Talent Support Program by China Association for Science and Technology (Grant 2016QNRC001).

References

Akiyama T (1973) The large-scale aspects of the characteristic features of the Baiu front. Pap Meteorol Geophys 24(2):157–188

Cao J, Huang RH, Xie Y, Tao Y (2002) The physical mechanism of evolution about the western Pacific subtropical high (in Chinese). Sci Sin Terrae 32(8):659–666

Chang CP (2004) East Asian Monsoon. World Scientific, Singapore, p 564

Chen TJ (1983) Observational aspects of the Mei-Yu phenomena in subtropical China. J Meteorol Soc Jpn 61:306–312

Chen TJ, Chang CP (1980) The structure and vorticity budget of an early summer monsoon trough (Mei-Yu) over southeastern China and Japan. Mon Weather Rev 108:942–953. https://doi.org/10.1175/1520-0493(1980)108<0942:TSAVBO>2.0.CO;2

Chen TJ, Yu CC (1988) Study of low-level jet and extremely heavy precipitation over northern Taiwan in the

Mei-Yu season. Mon Weather Rev 116:884–891. https://doi.org/10.1175/1520-0493(1988)116<0884:SOLLJA>2.0.CO;2
Choi KS, Wang B, Kim DW (2012) Changma onset definition in Korea using the available water resources index and its relation to the Antarctic oscillation. Clim Dyn 38:547–562. https://doi.org/10.1007/s00382-010-0957-1
Dai XG, Chou JF, Wu GX (2002) The teleconnection relationship between Indian monsoon and East Asian summer circulation. Acta Meteorol Sin 60(5):544–552
Ding YH (1992) Summer monsoon precipitations in China. J Meteorol Soc Jpn 70:373–396
Ding YH, Liu YJ, Sun Y, (2007) A Study of the Synoptic-Climatology of the Meiyu System in East Asia (in Chinese with English abstract). Chin J Atmos Sci 31(6)
Feng X, Dong X, Lin RP (2017) Two anomalous convective systems in the tropical western Pacific and their influences on the East Asian summer monsoon. Atmos Ocean Sci Lett 10(4):319–324. https://doi.org/10.1080/16742834.2017.1328969
Graversen RG, Burtu M (2016) Arctic amplification enhanced by latent energy transport of atmospheric planetary waves. Q J R Meteorol Soc 142(698):2046–2054
Hsu HH, Lin SM (2007) Asymmetry of the tripole rainfall pattern during the East Asian summer. J Clim 20:4443–4458. https://doi.org/10.1175/JCLI4246.1
Huang RH (1992) The East Asia/Pacific pattern teleconnection of summer circulation and climate anomaly in East Asia. J Meteorol Res 6:25–37
Huang YY, Li XF (2015) The interdecadal variation of the Western Pacific subtropical high as measured by 500 hPa Eddy geopotential height. Atmos Ocean Sci Lett 8(6):371–375. https://doi.org/10.3878/AOSL20150038
Huang DQ, Masaaki T, Zhang YC (2011) Analysis of the Baiu precipitation and associated circulations simulated by the MIROC coupled climate system model. J Meteorol Soc Jpn 89:625–636. https://doi.org/10.2151/jmsj.2011-603
Huang YY, Wang HJ, Fan K, Gao YQ (2014) The western Pacific subtropical high after the 1970s: westward or eastward shift? Clim Dyn 44(7–8):2035–2047
Huangfu JL, Huang RH, Chen W (2015) Influence of tropical western Pacific Warm Pool thermal state on the interdecadal change of the onset of the South China Sea Summer Monsoon in the Late-1990s. Atmos Ocean Sci Lett 8(2):95–99. https://doi.org/10.3878/AOSL20150002
Kalnay E et al (1996) The NCEP/NCAR 40-year reanalysis project. Bull Am Meteorol Soc 77:437–471
Kodama YM (1992) Large-scale common features of subtropical precipitation zones (the Baiu frontal zone, the SPCZ, and the SACZ). Part I: characteristics of subtropical frontal zones. J Meteorol Soc Jpn 70:813–836
Krishnan K, Sugi M (2001) Notes and correspondence Baiu rainfall variability and associated monsoon teleconnections. J Meteorol Soc Jpn 79:851–860
Kurihara K, Tsuyuki T (1987) Development of the barotropic high around Japan and its association with Rossby wave-like propagations over the North Pacific: analysis of August 1984. J Meteorol Soc Jpn Ser II 65(2):237–224
Lau KM, Yang GJ, Shen SH (1988) Seasonal and intraseasonal climatology of summer monsoon precipitation over East Asia. Mon Weather Rev 116:18–37. https://doi.org/10.1175/1520-0493(1988)116<0018:SAICOS>2.0.CO;2
Li L, Zhang YC (2014) Effects of different configurations of the East Asian subtropical and polar front jets on precipitation during the Mei-Yu season. J Clim 27(17):6660–6672. https://doi.org/10.1175/JCLI-D-14-00021.1
Liebmann B, Smith CA (1996) Description of a complete (interpolated) outgoing longwave radiation dataset. Bull Am Meteorol Soc 77:1275–1277
Liu YM, Wu GX, Liu H, Liu P (2001) Condensation heating of the Asian summer monsoon and the subtropical anticyclone in the Eastern Hemisphere. Clim Dyn 17(4):327–338
Liu YY, Li WJ, Ai WX, Li QQ (2012) Reconstruction and application of the monthly Western Pacific Subtropical High indices (in Chinese with English abstract). J Appl Meteorol Sci 23(4):414–423
Lu RY (2001) Interannual variability of the summertime north pacific subtropical high and its relation to atmospheric convection over the warm pool. J Meteorol Soc Jpn 79(3):771–783
Lu RY, Dong BW (2001) Westward extension of north Pacific subtropical high in summer. J Meteorol Soc Jpn 79(6):1229–1241
Lu RY, Oh JH, Kim BJ, Beak HJ, Huang RH (2001) Associations with the interannual variations of onset and withdrawal of the Changma. Adv Atmos Sci 18(6):1066–1080
Mao JY, Zhang S, Wu GX (2010) 20–50-day oscillation of summer Yangtze rainfall in response to intraseasonal variations in the subtropical high over the western north Pacific and South China Sea. Clim Dyn 34(5):747–761. https://doi.org/10.1007/s00382-009-0628-2
Nakamura H, Tanaka M, Wallace JM (1987) Horizontal structure and energetics of Northern Hemisphere wintertime teleconnection patterns. J Atmos Sci 44:3377–3391. https://doi.org/10.1175/1520-0469(1987)044,3377:<HSAEON>2.0.CO;2
Ninomiya K, Shibagaki Y (2007) Multi-scale features of the Meiyu-Baiu front and associated precipitation systems. J Meteorol Soc Jpn 85B:103–122
Nitta T, Hu ZZ (1996) Summer climate variability in China and its association with 500 hPa height and tropical convection. J Meteorol Soc Jpn 74:425–445
North GR, Bell TL, Cahalan RF, Moeng FJ (1982) Sampling errors in the estimation of empirical orthogonal functions. Mon Weather Rev 110:699–706
Ou SS, Liou KN, Liou WJ (1989) The seasonal cycle of the global zonally averaged energy balance. Theoret Appl Climatol 40(1–2):9–23
Park H, Seo KH, Son JH (2015) Development of a dynamics-based statistical prediction model for the Changma onset. J Clim 28:6647–6666. https://doi.org/10.1175/JCLI-D-14-00502.1
Reiter ER, Gao DY (1982) Heating of the Tibet Plateau and movements of the South Asian High during spring. Mon Weather Rev 110(11):1694–1711
Sampe T, Xie SP (2010) Large-scale dynamics of the Meiyu–Baiu rainband: environmental forcing by the westerly jet. J Clim 23:113–134
Tao SY, Chen LX (1987) A review of recent research on the East Asia summer monsoon in China. In: Chang CP, Krishnamurti TN (eds) Monsoon meteorology. Oxford University Press, Oxford, pp 60–92
Wakazuki Y, Tsuboki K, Takeda T (2006) Periodic evolution of multi-scale precipitation systems developed within a Baiu frontal cloud cluster. J Meteorol Soc Jpn 84:497–518
Wang B (1992) The vertical structure and development of the ENSO anomaly mode during 1979–1989. J Atmos Sci 49:698–712
Wang HJ, He SP (2015) The north China/Northeastern Asia severe summer drought in 2014. J Clim 28(17):6667–6681. https://doi.org/10.1175/JCLI-D-15-0202.1
Wang WZ, Zhao ZC, Gong DY, Zhou TJ (2005) Introduction of climatology. China Meteorological Press, Beijing, p 43
Wang B et al (2008) How to measure the strength of the East Asian Summer Monsoon. J Clim 21(17):4449–4463
Wen M, Shi XH (2006) Relationship between activity of west Pacific subtropical high and condensation latent heating in summer

of 1998 (in Chinese with English abstract). Plateau Meteorol 25(4):616–623

Xie PP, Arkin PA (1996) Analyses of global monthly precipitation using gauge observations, satellite estimates, and numerical model predictions. J Clim 9:840–858. https://doi.org/10.1175/1520-0442(1996)009,0840:AOGMPU.2.0.CO;2

Xu ZQ, Fan K, Wang HJ (2016) Role of sea surface temperature anomalies in the tropical Indo-Pacific region in the northeast Asia severe drought in summer 2014: month-to-month perspective. Clim Dyn 49:1631–1650. https://doi.org/10.1007/s00382-016-3406-y

Yanai M, Esbensen S, Chu JH (1973) Determination of bulk properties of tropical cloud clusters from large-scale heat and moisture budgets. J Atmos Sci 30:611–627. https://doi.org/10.1175/1520-0469(1973)030,0611:DOBPOT.2.0.CO;2

Yeh TC, Tao SY, Li MT (1959) The abrupt change of circulation over the Northern Hemisphere during June and October. In: Bolin B (ed) The atmosphere and the sea in motion. Rockefeller Institute Press, New York, pp 249–267

Yu F, Fu SM, Zhao SX, Sun JH (2012) Study on the dynamic characteristics of an eastward-offshore mesoscale vortex along the Meiyu-Baiu Front. Atmos Ocean Sci Lett 5:360–366

Zhang YX, Zhai PM, Qian YF (2005) Variations of Meiyu indicators in the Yangtze-Huaihe River basin during 1954–2003. Acta Meteorol Sin 19(4):479–484

Zhou TJ, Gong DY, Li J, Li B (2009) Detecting and understanding the multi-decadal variability of the East Asian summer monsoon—recent progress and state of affairs. Meteorol Z 18:455–467. https://doi.org/10.1127/0941-2948/2009/0396

Zhu X, Wu Z, He J (2008) Anomalous Meiyu onset averaged over the Yangtze River valley. Theor Appl Climatol 94:81–95. https://doi.org/10.1007/s00704-007-0347-8

Zhu YL, Wang HJ, Zhou W, Ma JH (2011) Recent changes in the summer precipitation pattern in East China and the background circulation. Clim Dyn 36:1463–1473. https://doi.org/10.1007/s00382-010-0852-9

Zhu J et al (2013) Decadal changes of Meiyu rainfall around 1991 and its relationship with two types of ENSO. J Geophys Res 118:9766–9777. https://doi.org/10.1002/jgrd.50779

Zhu YL, Wang HJ, Ma JH, Wang T, Sun JQ (2015) Contribution of the phase transition of Pacific Decadal Oscillation to thelast1990s' shift in East China summer rainfall. J Geophys Res 120:8817–8827. https://doi.org/10.1002/2015JD023545